Available online at www.sciencedirect.com
ScienceDirect
Journal of the European Ceramic Society 28 (2008) 929–934
www.elsevier.com/locate/jeurceramsoc

Texturing behavior in sintered reaction-bonded silicon nitride via strong magnetic field alignment

Xinwen Zhu, Tohru S. Suzuki, Tetsuo Uchikoshi, Yoshio Sakka *

Nano Ceramics Center, National Institute for Materials Science, 1-2-1, Sengen, Tsukuba, Ibaraki 305-0047, Japan

Available online 22 October 2007

Abstract

An attempt has been made to study the texture behavior in sintered reaction-bonded silicon nitride by strong magnetic field alignment, using slip casting of Si-powder without and with β-Si_3N_4 particle addition. It is shown that the *a*, *b*-axis aligned texture, parallel to the magnetic field, develop in the resultant SRBSN with β-seed addition, whereas no texture develops in those SRBSN without β-seed addition. The degree of orientation of β-Si_3N_4 is found to decrease with the formation of new β-phase during the nitridation, regardless of the nitriding conditions, suggesting that the initially oriented β-seed dose not promote the formation of newly oriented β-Si_3N_4. Compared to the nitridation, the degree of texture is enhanced by the post-sintering, but the nitridation condition has little effect on the texture development during the post-sintering. The present work implies that the texture development in SRBSN is governed by the initial orientation of β-Si_3N_4 seed and the post-sintering.

Keywords: Slip casting; Sintering; Microstructure-final; Si_3N_4; Texture

1. Introduction

Sintered reaction-bonded silicon nitride (SRBSN) is a well-known cost-effective Si_3N_4 ceramic material because of the cheaper Si raw powder, the 60% weight gains from silicon nitridation, machinability of RBSN body and lower sintering shrinkage.[1–3] SRBSN is typically produced by a two-step process: nitridation and post-sintering. The nitridation allows the Si compact with a density of ∼60% theoretical to produce the porous RBSN body with a density of 70–80% theoretical as a result of the 22 vol% expansion. The post-sintering enables the porous RBSN body with higher density to reach full densification at the lower shrinkage and lower distortion. Recent studies showed that in addition to the low-cost benefit, SRBSN possess the potential capacity of producing Si_3N_4 components with comparable thermal and mechanical properties to those with the direct sintering of Si_3N_4 powder.[4–7] In addition to the cost, the limited properties also hinder the widespread applications of Si_3N_4 ceramics. It is expected that the texturing of SRBSN is helpful to expand the applications of Si_3N_4 ceramics because of the improved properties, such as mechanical properties, thermal conductivity, tribological properties, etc.[8]

One popular method of texturing Si_3N_4 is the so-called "templated grain growth (TGG)", which involves the alignment of a small amount of large β-Si_3N_4 seed particles in a fine powder matrix by tape casting[9] or extrusion.[10] The subsequent sintering allows the template grains to grow anistropically and abnormally, resulting in the textured microstructure with the grain alignment parallel to the casting or extrusion direction. Another popular method is the hot-working, which involves the imposition of a uniaxial stress to rotate the elongated grains during the sintering or superplastic deformation (e.g. hot-pressing, sintering forging and superplastic deformation),[11] resulting in the textured microstructure with the grain alignment parallel or perpendicular to the plane strain, depending on the tensile or compressive strain. Recently, strong magnetic field alignment (hereafter SMFA) has been developed to texture "non-magnetic" ceramics (e.g. Al_2O_3, TiO_2, AlN, Si_3N_4, etc.), which involves the alignment of the particles in a strong magnetic field typical of ≥10 T during slurry consolidation, followed by sintering.[12–15] The alignment is achieved with the axis showing highest magnetic susceptibility parallel to the magnetic field. For this method, the key requirements are: (i) the material should exhibit magnetic anisotropy; (ii) the magnetic field is strong enough to provide an anisotropic magnetic energy higher than thermal motion energy and (iii) the suspension should be well dispersed with low viscosity. One important attraction of SMFA is the independence of the grain morphology, and its

* Corresponding author. Tel.: +81 29 859 2461; fax: +81 29 859 2401.
E-mail address: SAKKA.Yoshio@nims.go.jp (Y. Sakka).

0955-2219/$ – see front matter © 2007 Elsevier Ltd. All rights reserved.
doi:10.1016/j.jeurceramsoc.2007.09.019

applicability to the very fine grains even at nano-scale size. Another attraction is the versatility and simplicity of the fabrication process, because various colloidal forming approaches are well developed, such as slip casting, electrophoretic deposition, gel casting, etc.

Previous studies demonstrated that owing to the magnetic susceptibility of $\chi_{a,b} > \chi_c$, the *a*, *b*-axis aligned β-Si_3N_4 can be produced by slip casting of α-Si_3N_4 raw powder in a strong magnetic field of ≥10 T, followed by pressureless sintering,[16,17] but the alignment of minor β-phase in the α-powder plays an important role in the development of textured β-Si_3N_4,[17] because the crystallographic orientation of β-Si_3N_4 is probably disturbed by the α → β phase transformation that occurs through the solution-reprecipitation process. As the nitridation of Si is a nucleation and grain growth process,[18] the aligned β-Si_3N_4 seed particles, induced by SMFA during slip casting, probably favor the formation of the aligned β-Si_3N_4 products during the nitridation of Si compacts. The post-sintering further enhances the texture development of SRBSN (β-Si_3N_4) via the α → β phase transformation and grain growth. Therefore, the present work is to conduct a preliminary study of the texturing behavior in SRBSN by SMFA, using non-aqueous slip casting, followed by nitriding at 1400–1450 °C and subsequent post-sintering at 1800 °C in nitrogen atmosphere.

2. Experimental procedure

A type of fine Si powder (MSi No. 600, d_{50} = 2 μm, Yamaishi Metal Co., Ltd., Tokyo, Japan, 0.39 wt% Fe and 0.1 wt% Al) was used as the starting powder, and β-Si_3N_4 powder (NP-500, 3.4 wt% α-Si_3N_4, d_{50} = 0.63 μm, Denki Kagaku Kogyo Co., Tokyo, Japan) was used for seeding. A mixture of Y_2O_3 (purity > 99.9%, Shin-Etsu Chemicals, Tokyo, Japan) and MgO (1000A, UBE Industries, Ltd., Yamaguchi, Japan) was used as sintering additives, because it allows SRBSN to show higher thermal conductivity.[19] The crystal orientation in green and sintered bodies was evaluated by X-ray diffractometry (XRD). The morphology of the Si and β-Si_3N_4 raw powders is presented in Fig. 1. It is clear that the Si particles have irregular shapes with sharp corners and exhibit a very wide particle size distribution, showing the largest particles with size of up to 20 μm. In β-Si_3N_4 powder, most of β-Si_3N_4 particles are less agglomerated with irregular shapes, enabling them to align easily during slip casting in the magnetic field, because only single crystal particle is operated for the alignment induced by the magnetic field. The composition of Si compacts was determined based on the composition after full nitridation as Si_3N_4:Y_2O_3:MgO = 90:5:5 at molar ratio. Converted to the weigh percentage, the composition was 90.47% Si_3N_4 + 8.09% Y_2O_3 + 1.44% MgO. The amount of β-Si_3N_4 powder used was fixed at 5% in weight based on the total weight after full nitridation. The samples without and with β-Si_3N_4 seed addition were designated as RYM and RYMS, respectively.

Ethanol was used as a solvent and polyethylenimine (PEI) (M_W = 10 000 g mol^{-1}, Wako Pure Chemical Industries, Ltd., Tokyo, Japan) was used as a dispersant. The amount of PEI was fixed at 1 wt% based on the total weight of powders. The 30 vol% slurry was prepared by planetary milling for 2 h in a Si_3N_4 jar with Si_3N_4 balls. After degassing, slip casting was performed using a glass case set on the porous Al_2O_3 block with a type of 0.2 μm membrane filter in the magnetic field of 12 T. The direction of magnetic field was parallel to the direction of slip casting. After consolidation, the drying was done in a vacuum oven at 110 °C, followed by cold isostatic pressing at 300 MPa. The green bodies were calcined at 500 °C for 2 h in air to burn out the polymer dispersant prior to the nitridation. Based on the apparent dimension and weight, the samples RYM and RYMS were estimated to show a green density of ~58% theoretical. The calcined samples were placed on a powder bed composed of only BN powder in a graphite crucible. The nitridation was conducted in a graphite-resistance furnace at 1400–1450 °C with 2 L/min nitrogen flow. The nitrided samples were embedded in a power bed composed of only BN powder in a graphite crucible. The sintering was conducted in the same graphite-resistance furnace at 1800 °C for 1 h under a nitrogen pressure of 0.2 MPa.

The nitrided and sintered samples were cut in directions parallel and perpendicular to the imposed magnetic field. The phase

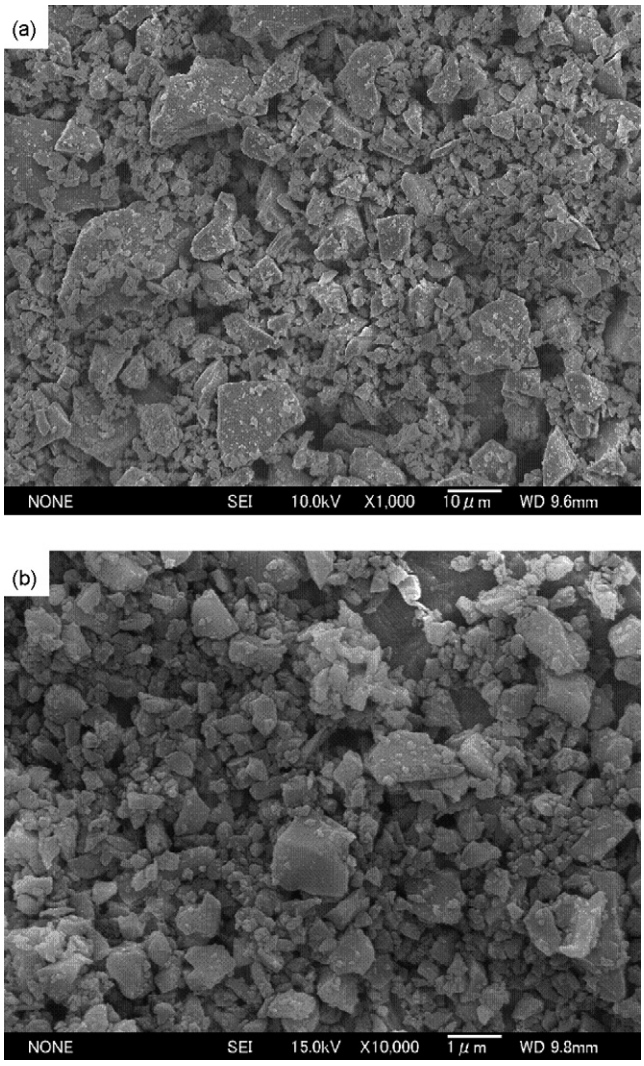

Fig. 1. SEM micrographs of (a) Si and (b) β-Si_3N_4 raw powders used in this study.

and crystallographic orientation analysis was conducted on the each surface of the samples using XRD (Model RINT 2500, Rigaku Co., Tokyo, Japan, Cu Kα radiation, 40 kV ∼ 300 mA). The quantitative analysis of α- and β-Si_3N_4 of the nitrided samples was performed using the diffraction intensities of the (1 0 1), (2 0 1), (1 0 2) and (3 0 1) planes for α-Si_3N_4, and of the (1 1 0), (2 0 0), (1 0 1) and (2 1 0) planes for β-Si_3N_4, according to the method developed by Gazzara and Messier.[20]

3. Results and discussion

Fig. 2 gives the XRD patterns of the top and side surfaces of green samples RYM and RYMS. In sample RYM, no difference is observed in the diffraction peak intensities of Si between the top and side surfaces, as shown in Fig. 2(a). This indicates that the magnetic field does not lead to the alignment of Si particles, which is consistent with the cubic structure of Si, suggesting the magnetic isotropy. The crystallographic orientation of MgO is not considered here, because its role is to participate in the formation of the liquid phase and does not affect the crystallographic orientation of β-Si_3N_4. Although the role of Y_2O_3 is the same as MgO, some of its diffraction peaks overlap with those of β-Si_3N_4, thereby affecting the evaluation of the crystallographic orientation of β-Si_3N_4 seed particles. Therefore, the diffraction data of Y_2O_3 is needed to be analyzed in sample RYM without β-seed addition. For Y_2O_3, on the top and side surfaces, the ratios

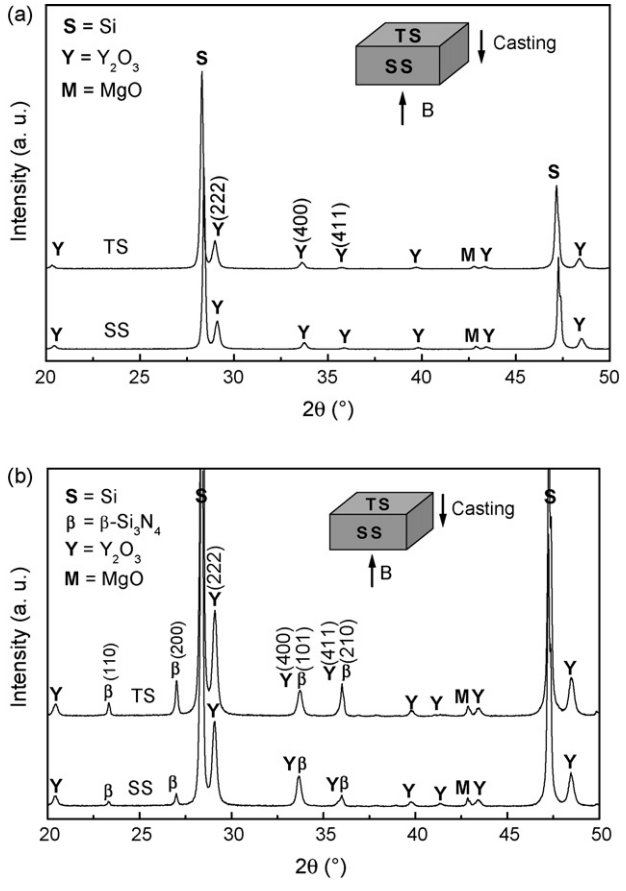

Fig. 2. XRD patterns of the green samples (a) RYM and (b) RYMS (TS = top surface ⊥ B, SS = side surface // B).

of the peak intensities of the (4 0 0) and (2 2 2), and (4 1 1) and (2 2 2) planes, $I_{(400)}/I_{(222)}$ and $I_{(411)}/I_{(222)}$, are determined to be 0.23 and 0.05, respectively. This is in agreement with the data of standard JCPDS card No. 41-1105, showing that the values of $I_{(400)}/I_{(222)}$ and $I_{(411)}/I_{(222)}$ are 0.24 and 0.05, respectively. This clearly indicates that the magnetic field does not lead to the crystallographic orientation of Y_2O_3 during slip casting because of the cubic structure.

In sample RYMS, it is obviously found that the diffraction peaks of the ($h\,k\,0$) planes of β-Si_3N_4, typical of (1 1 0), (2 0 0) and (2 1 0) planes parallel to the *a*, *b*-axis of the unit cell, show substantially stronger relative intensities on the top surface than on the side surface. But, the diffraction peak of the (1 0 1) plane intersecting the *c*-axis show a change from the week relative intensity on the top surface to the strongest one among the diffractions of β-Si_3N_4 on the side surface. This indicates that the strong magnetic filed leads to the crystallographic orientation of β-Si_3N_4 with *a*, *b*-axis parallel to the magnetic field, as was demonstrated previously. Considering that the diffraction peak of the (0 0 2) plane ($2\theta \approx 64°$) is too weak to be distinguished, we use the ratio of the peak intensities of the (2 1 0) and (1 0 1) planes, $I_{(210)}/I_{(101)}$, to qualitatively evaluate the degree of texture of β-Si_3N_4 in the samples. [21] Although the (4 0 0) and (4 1 1) peaks of Y_2O_3 overlap with the (1 0 1) and (2 1 0) peaks of β-Si_3N_4, respectively, Y_2O_3 does not show crystallographic orientation. According to the diffraction data of Y_2O_3 in sample RYM, therefore, the value of $I_{(210)}/I_{(101)}$ for β-Si_3N_4 in sample RYMS can be calculated by the following way:

$$\frac{I_{(210)}}{I_{(101)}} = \frac{I_{\text{total},2\theta\cong 36°} - I_{Y_2O_3(411)}}{I_{\text{total},2\theta\cong 33.7°} - I_{Y_2O_3(400)}} = \frac{I_{\text{total},2\theta\cong 36°} - I_{Y_2O_3(222)} \times 0.05}{I_{\text{total},2\theta\cong 33.7°} - I_{Y_2O_3(222)} \times 0.23} \quad (1)$$

As shown in Table 1, the value of $I_{(210)}/I_{(101)}$ is found to show a large decrease from 20.97 on the top surface to 0.66 on the side surface, suggesting a very strong orientation. This further indicates that the strong magnetic field of 12 T is very efficient to align the β-Si_3N_4 particles in suspension.[17]

XRD analysis reveals that both samples RYM and RYMS exhibits complete nitridation at the temperatures of 1400 and 1450 °C, and the ratio of α- and β-phases depends on the sample and nitriding temperature. Table 2 shows the β/(α + β) ratios determined by XRD analysis of the top and side surfaces of the bulk samples. Clearly, sample RYMS exhibits substantially higher β/(α + β) ratio than sample RYM in all cases, indicating that the addition of β-Si_3N_4 seed promotes significantly the formation of β-phase during the nitridation. The enhanced β-phase formation is attributed to the "seeding" effect of β-Si_3N_4 addition. It is generally accepted that the nitridation of Si is a "nucleation and growth of Si_3N_4" process,[18] in which the addition of α-Si_3N_4 promotes the formation of α-phase, whereas the addition of β-Si_3N_4 promotes the formation of β-phase.[3,22,23] In addition, at 1450 °C/24 h the β/(α + β) ratios in both samples RYM and RYMS increases largely to higher than 70 and 90 wt% in comparison with those at 1400 °C/8 h, respectively. This indicates that the formation of β-phase is significantly promoted by

Table 1
Crystallographic orientation identified by XRD for β-Si_3N_4 crystals in the green, nitrided (RBSN) and post-sintered (SRBSN) samples

Sample	Tested surface[a]	XRD intensity ratio of $I_{(2\,1\,0)}/I_{(1\,0\,1)}$ for β-Si_3N_4[b]				
		Green	RBSN		SRBSN (1800 °C-1 h)	
			1400 °C-8 h	1450 °C-24 h	Nitriding at 1400 °C-8 h	Nitriding at 1450 °C-24 h
RYM	TS	–	0.84	0.85	0.59	0.72
	SS	–	1.02	1.04	0.80	0.82
	TS/SS[c]	–	0.82	0.82	0.74	0.88
RYMS	TS	20.97	1.73	1.63	3.42	3.05
	SS	0.66	0.74	0.79	0.49	0.50
	TS/SS[c]	31.77	2.34	2.06	6.98	6.10

[a] TS = top surface ⊥ B, SS = side surface // B.
[b] $I_{(2\,1\,0)}/I_{(1\,0\,1)}$ = 0.94 from standard JCPDF card (No. 33-1160) of β-Si_3N_4.
[c] The ratio of the $I_{(2\,1\,0)}/I_{(1\,0\,1)}$ value between the top and side surfaces was defined as the orientation factor to evaluate the degree of orientation of β-Si_3N_4.

the nitriding temperature higher than the melting point of Si (1410 °C). This is attributed to the nitridation of molten Si and the α–β phase transformation, because the nitridation of molten Si tends to form β-Si_3N_4, and the α–β phase transformation also produces only β-Si_3N_4 through the liquid Si and/or intergranular liquid phase, [22,24,25] where α-Si_3N_4 dissolves and precipitates as β-Si_3N_4, the co-called "dissolution-precipitation" process. Moreover, it is interesting to see that in sample RYM, there is almost no difference in the β/(α + β) ratio between the top and side surfaces, whereas in sample RYMS, the β/(α + β) ratio is higher on the top surface than on the side surface. This phenomenon is related to the orientation of β-Si_3N_4 grains in sample RYMS.

Table 1 shows the values of $I_{(2\,1\,0)}/I_{(1\,0\,1)}$ of β-Si_3N_4 identified by XRD in the nitrided samples RYM and RYMS at different nitriding conditions. Because of the negligible orientation, sample RYM shows very small difference in the $I_{(2\,1\,0)}/I_{(1\,0\,1)}$ value between the top and side surfaces. However, sample RYMS shows a large decrease in the $I_{(2\,1\,0)}/I_{(1\,0\,1)}$ value from the top and side surfaces. To understand the texture development, we further use the ratio of the $I_{(2\,1\,0)}/I_{(1\,0\,1)}$ value between the top and side surfaces as orientation factor to evaluate the degree of orientation of β-Si_3N_4 in sample RYMS. As shown in Table 1, the nitridation leads to a dramatic decrease in the orientation factor from 31.77 to 2.34, despite the large increase in the β-Si_3N_4 content from 5 to 55 wt%. The β-Si_3N_4 content was based on the total weight of the samples, estimated from the average value between the top and side surface (Table 2), and the nominal composition (90.47% Si_3N_4 + 8.09% Y_2O_3 + 1.44% MgO at weight). This indicates that the newly formed β-Si_3N_4 significantly reduce the degree of orientation during the nitridation. When the β-Si_3N_4 content increases up to 85 wt% after nitriding at 1450 °C/24 h, the orientation factor further shows a slight decrease. The results suggest that the oriented β-Si_3N_4 seed does not result in the crystallographic orientation of the newly formed β-Si_3N_4 grain from the nitridation of Si particles, despite the promoted β-Si_3N_4 formation, i.e., the formation of the more amount of randomly oriented β-Si_3N_4 phase during the nitridation leads to a decrease in the degree of orientation of β-Si_3N_4. Šajgalík et al.[26] also observed a decrease in the degree of orientation of β-Si_3N_4 in hot-pressed SiC/Si_3N_4 nano/micro-composite with prolonged high-temperature annealing, and they attributed the reason to the exaggerated grain growth of randomly oriented β-Si_3N_4 grains.

Table 2
The β/(α + β) ratios in the nitrided samples RYM and RYMS

Sample	Tested surface	β/(α + β) (wt%)	
		1400 °C-8 h	1450 °C-24 h
RYM	TS	29.90	74.43
	SS	30.32	72.83
RYMS	TS	66.01	95.83
	SS	55.96	92.35

After post-sintering at 1800 °C for 1 h, the α–β phase transformation is completed in all cases, as demonstrated by XRD analysis. Owing to the untextured development, sample RYM shows almost no difference in the XRD patterns of β-Si_3N_4 between the top and side surfaces. However, sample RYMS shows substantially stronger relative intensities of all ($h\,k\,0$) diffraction peaks of β-Si_3N_4 on the top surface than on the side surface. Particularly, the diffraction peaks of the (1 0 1) and (0 0 2) planes are relatively weak on the top surface, but they become relatively stronger on the side surface. This indicates that the texture with the *a*, *b*-axis parallel to the magnetic field develops in the post-sintered sample RYMS. The crystallographic orientation identified by XRD for the β-Si_3N_4 crystals in the post-sintered samples is also shown in Table 1. The post-sintering leads to a large decrease in the orientation factor by three times, compared to the nitrided cases. It is interesting to see that the nitriding condition has little effect on the degree of orientation in SRBSN, despite resulting in the largely different β-phase content. Despite this, the degree of orientation of β-Si_3N_4 is substantially lower in the SRBSN samples than in the green samples. Fig. 3 summarizes the orientation factor in the green, nitrided and post-sintered RYMS. It illustrates that during the nitridation, the formation of randomly aligned β-Si_3N_4 product considerably reduces the degree of orientation because of the mixing effect, and during the post-sintering at higher temperature, the degree of orientation is enhanced because of the promoted β-Si_3N_4 grain growth, typical of the anisotropic

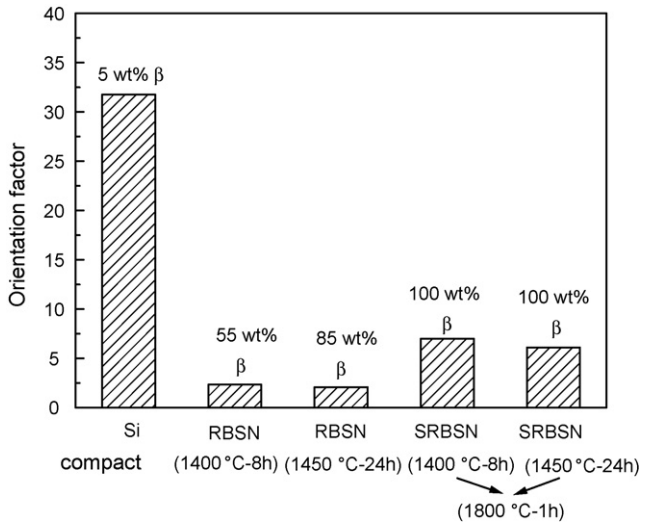

Fig. 3. Orientation factor of β-Si_3N_4 in the green, nitrided and post-sintered sample RYMS. The orientation factor is defined as the ratio of the $I_{(2\,1\,0)}/I_{(1\,0\,1)}$ value between the top and side surfaces, perpendicular and parallel to the magnetic field, respectively.

grain growth. Moreover, Fig. 4 plots the orientation factor as a function of the volume fraction of β-Si_3N_4 seed in the nitrided sample RYMS, which suggests that the degree of orientation of β-Si_3N_4 decreases with the formation of β-phase product during the nitridation of Si compact.

Furthermore, the Lotgering orientation factor, f, was used to evaluate the degree of texture in the post-sintered samples RYMS, according to the equation: [27]

$$f = \frac{P - P_0}{1 - P_0} \tag{2}$$

$$P \text{ and } P_0 = \frac{\sum I_{(h\,k\,0)}}{\sum I_{(h\,k\,l)}} \tag{3}$$

where $\sum I_{(h\,k\,0)}$ and $\sum I_{(h\,k\,l)}$ are the sums of the $(h\,k\,0)$ and $(h\,k\,l)$ intensities in the range of 2θ from 10 to 70°. The values of P were calculated from the measured XRD data of β-Si_3N_4 on the top surfaces of the post-sintered samples, and the values of P_0 were calculated from the data of the standard JCPDS card No. 33-1160 of β-Si_3N_4. The f values of the post-sintered samples obtained from the nitrided bodes at 1400 °C-8 h and 1450 °C-24 h are determined to be 0.52 and 0.46, respectively. This result also suggests that the nitriding condition has no significant effect on the texture development in SRBSN during the post-sintering. As the texture development during the post-sintering is associated with the growth of the initially aligned β-Si_3N_4 seed, similar to the mechanism in TGG, [8–10,17] the texture in SRBSN can be enhanced by controlling the β-Si_3N_4 seed (size, amount and dispersion) and the post-sintering (temperature and time).

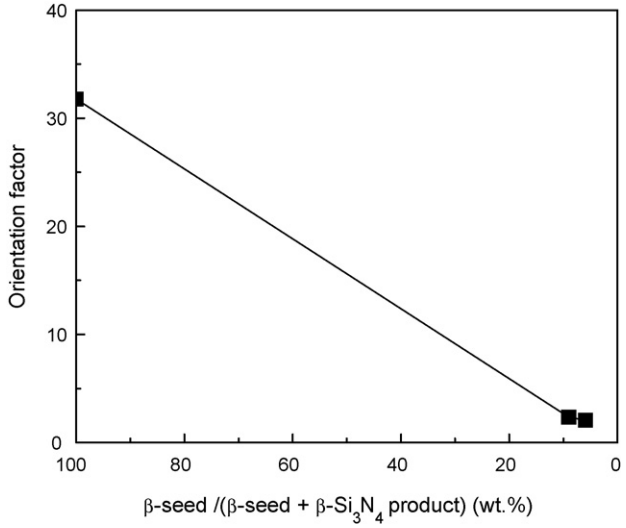

Fig. 4. Orientation factor vs. the weight fraction of β-seed in the nitrided sample RYMS.

4. Conclusions

Aligned SRBSN has been obtained by strong magnetic field alignment (SMFA), using slip casting of Si-powder seeded with β-Si_3N_4 particles. It was found that the degree of orientation of β-Si_3N_4 decreases with the formation of new β-phase during the nitridation regardless of the nitriding conditions, suggesting that the initially oriented β-seed dose not promote the formation of newly oriented β-Si_3N_4. Compared to the nitridation, the degree of texture is enhanced by the post-sintering, but the nitridation condition has little effect on the texture development during the post-sintering. The present work implies that the texture development in SRBSN is governed by the initial orientation of β-Si_3N_4 seed and the post-sintering.

References

1. Mangels, J. A. and Tennenhouse, G. J., Densification of reaction-bonded silicon nitride. *Am. Ceram. Soc. Bull.*, 1980, **59**, 1216–1218, 1222.
2. Tiegs, T. N., Kiggans, J. O. and Ploetz, Z. L., Cost-effective sintered reaction-bonded silicon nitride for structural ceramics. *Ceram. Eng. Sci. Proc.*, 1993, **14**, 378–388.
3. Tiegs, T. N., Kiggans, J. O., Montgomery, F. C., Lin, H. T., Barker, D. L., Snodgrass, J. D. *et al.*, Effect of composition on the processing and properties of sintered reaction-bonded silicon nitride. *Ceram. Eng. Sci. Proc.*, 1996, **17**, 354–362.
4. Lee, B. T., Yoo, J. H. and Kim, H. D., Microstructure characterization of GPSed-RBSN and GPSed-Si_3N_4 ceramic. *Mater. Trans.*, 2000, **41**, 312–316.
5. Lee, J. S., Mun, J. H., Han, B. D. and Kim, H. D., Effect of β-Si_3N_4 Seed Particles on the Property of Sintered Reaction-Boned Silicon Nitride. *Ceram. Int.*, 2003, **29**, 897–905.
6. Zhu, X. W., Sakka, Y., Zhou, Y. and Hirao, K., Processing and properties of sintered reaction-bonded silicon nitride with Y_2O_3-$MgSiN_2$: effects of Si powder and Li_2O addition. *Acta Mat.*, 2007, **55**, 5581–5591.
7. Zhu, X. W., Zhou, Y., Hirao, K. and Lenčéš, Z., Processing and thermal conductivity of sintered reaction-bonded silicon nitride. I: Effect of Si powder characteristics. *J. Am. Ceram. Soc.*, 2006, **89**, 3331–3339.
8. Hirao, K., Microstructure control of silicon nitride ceramics by seeding and their enhanced mechanical and thermal properties. *J. Ceram. Soc. Jpn.*, 2006, **104**, 665–671.
9. Hirao, K., Ohashi, M., Brito, M. E. and Kanzaki, S., Processing strategy of producing highly anisotropic silicon nitride. *J. Am. Ceram. Soc.*, 1995, **78**, 1687–1690.
10. Muscat, D., Pugh, M. D. and Drew, R. A. L., Microstructure of an extruded β-silicon nitride whisker-reinforced silicon nitride composites. *J. Am. Ceram. Soc.*, 1992, **75**, 2713–2718.

11. Kondo, N., Suzuki, Y. and Ohji, T., Superplastic sinter-forging of silicon nitride with anisotropic microstructure formation. *J. Am. Ceram. Soc.*, 1999, **82**, 1067–1069.
12. Suzuki, T. S., Sakka, Y. and Kitazawa, T., Orientation amplification of alumina by colloidal filtration in a strong magnetic field and sintering. *Adv. Eng. Mater.*, 2001, **3**, 490–492.
13. Sakka, Y. and Suzuki, T. S., Textured development of feeble magnetic ceramics by colloidal processing under high magnetic field. *J. Ceram. Soc. Jpn.*, 2005, **113**, 26–36.
14. Suzuki, T. S. and Sakka, Y., Preparation of oriented bulk 5 wt% Y_2O_3-Al_2O_3 ceramics by slip casting in a high magnetic field and sintering. *Scripta Mater.*, 2005, **52**, 583–586.
15. Suzuki, T. S., Uchikoshi, T. and Sakka, Y., Control of texture in alumina by colloidal processing in a strong magnetic field. *Sci. Technol. Adv. Mater.*, 2006, **7**, 356–364.
16. Li, S. Q., Sassa, K. and Asai, S., Fabrication of textured Si_3N_4 ceramics by slip casting in a high magnetic field. *J. Am. Ceram. Soc.*, 2004, **87**, 1384–1387.
17. Zhu, X. W., Suzuki, T. S., Uchikoshi, T., Nishimura, T. and Sakka, Y., Texture development in Si_3N_4 ceramics by magnetic field alignment during slip casting. *J. Ceram. Soc. Jpn.*, 2006, **114**, 979–987.
18. Atkinson, A., Moulson, A. J. and Roberts, E. W., Nitridation of high-purity silicon. *J. Am. Ceram. Soc.*, 1976, **59**, 285–289.
19. Zhu, X. W., Zhou, Y., Hirao, K. and Lenčéš, Z., Processing and thermal conductivity of sintered reaction-bonded silicon nitride. II: Effects of magnesium compound and yttria additives. *J. Am. Ceram. Soc.*, 2007, **90**, 1684–1692.
20. Gazzara, C. P. and Messier, D. R., Determination of phase content of Si_3N_4 by X-Ray diffraction analysis. *Am. Ceram. Soc. Bull.*, 1977, **56**, 777–780.
21. Goto, Y., Ohta, H., Komatsu, M. and Komeya, K., Preferred orientation and mechanical properties of pressureless sintered silicon nitride. *Yogyo-Kyokai-Shi*, 1986, **94**, 167–171.
22. Morgan, P. E. D., The α/β-Si_3N_4 question. *J. Mater. Sci.*, 1980, **15**, 791–793.
23. Gregory, O. J. and Richman, M. H., The role of Si_3N_4 additions in the reaction bonding of silicon compacts. *J. Mater. Sci. Lett.*, 1984, **3**, 112–116.
24. Jennings, H. M., On reactions between silicon and nitrogen: Part 1. Mechanisms. *J. Mater. Sci.*, 1983, **18**, 951–967.
25. Park, J. Y., Kim, J. R. and Kim, C. H., Effects of free silicon on the α to β phase transformation in silicon nitride. *J. Am. Ceram. Soc.*, 1987, **70**, C-240–C-242.
26. Šajgalík, P., Hnatko, M., Lojanová, Š., Lenčéš, Z., Pálková, H. and Dusza, J., Microstructure, hardness, and fracture toughness evolution of hot-pressed SiC/Si_3N_4 nano/micro composite after high-temperature treatment. *Int. J. Mater. Res.*, 2006, **97**, 772–777.
27. Lotgering, F. K., Topotactical reactions with ferromagnetic oxides having hexagonal crystal structures—I. *J. Inorg. Nucl. Chem.*, 1959, **9**, 113–123.